Theoretical analysis of the coherence-brightened laser in air

Luqi Yuan,[1,2] Brett H. Hokr,[1] Andrew J. Traverso,[1] Dmitri V. Voronine,[1,2] Yuri Rostovtsev,[3]
Alexei V. Sokolov,[1] and Marlan O. Scully[1,2,4]
[1]*Texas A&M University, College Station, Texas 77843, USA*
[2]*Princeton University, Princeton, New Jersey 08544, USA*
[3]*University of North Texas, Denton, Texas 76203, USA*
[4]*Baylor University, Waco, Texas 76798, USA*
(Received 25 October 2012; published 20 February 2013)

We present a detailed theoretical study of a recent experiment [A. J. Traverso *et al.*, Proc. Natl. Acad. Sci. USA **109**, 15185 (2012)] in which a laserlike source is created in air by pumping with a nanosecond pulse. The source generates radiation in the forward and backward directions. The temporal behavior of the emitted pulses is investigated for different pump shapes and durations. Our analysis indicates that the spiky emission is due to quantum coherence via cooperation between atoms of an ensemble, which leads to strong-oscillatory superfluorescence. We show that these cooperative nonadiabatic coherence effects cannot be described by rate equations and instead a full set of the Maxwell-Bloch equations must be used. We consider a range of parameters and study transitions between various regimes. Understanding these coherence-brightened processes in air should lead to improvements in environmental, atmospheric remote sensing and other applications.

DOI: 10.1103/PhysRevA.87.023826 PACS number(s): 42.50.Gy, 42.50.Nn, 42.68.Ay

I. INTRODUCTION

Coherently generated optical signals have been widely investigated in the field of remote sensing as their high efficiency and directionality hold promise for environmental monitoring and chemical and biohazard detection. Backward-propagating coherent signals can be generated by focusing forward-propagating laser beams on a target in air [1–4] or through four-wave-mixing processes such as coherent anti-Stokes Raman scattering by focusing both forward and backward light sources [5,6]. The latter methods are simpler, but require a backward light source that propagates from the atmosphere to the ground. Generation of such backward lasing in air has been achieved recently by two-photon excitation of oxygen atoms using a picosecond forward-propagating pump pulse [7]. Another study has shown high-gain coherence-brightening behavior using a nanosecond pump pulse [8]. Therefore, the demonstration of a backward coherent light source in air provides an alternative possibility for atmospheric remote sensing via a coherently scattered signal. Here we present a detailed theoretical study of the collective emission observed in Ref. [8] and provide a better understanding of the nature of the coherence-brightened lasing in air.

The coherence-brightened laser, a superradiant source, can be realized from a pencil-shaped gain medium without mirrors as proposed by Dicke [9,10]. The Dicke superradiant pulse was first observed in optically pumped HF gas and studied using a semiclassical treatment [11,12]. Further study of the superradiant regime with a swept-gain excitation suggests interesting applications such as an x-ray laser source [13]. Superradiance and superfluorescence (SF) as the collective emission phenomena have been extensively studied and reviewed [14,15]. The main distinction between superradiance and SF is the initial coherence. In superradiance, the system is initially coherent, whereas in superfluorescence, the coherence builds up in an initially incoherent inverted medium.

Yoked superfluorescence (YSF) is another example of collective emission in a three-level cascade scheme [16,17]. Such a YSF-type system is prepared with a coherent two-photon excitation from the lower to the upper level. The transition between the upper and middle levels is accompanied by the emission of a SF pulse from an initially inverted configuration. This emission is coupled with the quantum coherence between the upper and lower levels and as a result, another pulse (namely, YSF) from the transition between the middle and lower levels is emitted. This process occurs only when all three fields are phase matched (for example, all three fields propagate in the forward direction). This three-level cascade system simultaneously emits a backward field from the upper transition; a backward field from the lower transition is not emitted because there is no population inversion there. This results in different emission behavior for the forward and backward fields [18,19].

There has been interest in coherence effects in lasing processes for decades [20–22]. It has been widely accepted that the coherent effects, which cannot be described by the rate equations, are present when the polarization evolves faster than or on the same time scale as the decoherence time [22,23]. The estimated average Rabi frequency for the emitted fields in the recent experiment [8] is higher than 10^{11} rad/s, which is significantly higher than the dephasing rate of 10^{10} s^{-1}. This provides evidence for the coherence effects.

Various regimes of N-atom cooperative spontaneous emission are defined by the values of several characteristic parameters [24] such as the single-pass gain [25]

$$\alpha L = \frac{2T_2}{\tau_r}, \tag{1}$$

where T_2 is the collisional dephasing time, the collective damping time [26]

$$\tau_r = \frac{8\pi}{3}\frac{T_1}{n\lambda^2 L}, \tag{2}$$

where T_1 is the spontaneous lifetime, λ is the wavelength, L is the gain length, and n is the excited atom density, the delay

time [27]

$$\tau_D = \tau_r \left[\tfrac{1}{4}\ln(2\pi N)\right]^2, \tag{3}$$

where $N = nAL$ is the total number of excited atoms in the gain volume (with the cross-sectional area A of the gain medium), and the cooperation number [28]

$$N_c = \frac{8\pi c T_1 A}{3\lambda^2 L} = N\frac{\tau_r c}{L}. \tag{4}$$

The physical meaning of each regime is discussed in detail in Ref. [24]. We summarize it briefly here. In the limit $T_2 \to \infty$, there is no collisional dephasing, so SF is radiated for the duration τ_r with a delay time of τ_D. In the regime $T_2 > \tau_D$, the coherence can be built up during the time τ_D before it decays by collisions and the cooperative emission process may occur. However, in the opposite regime where $T_2 < \sqrt{\tau_r \tau_D}$, the large collisional dephasing rate prevents coherence from building up. Thus the system generates amplified spontaneous emission (ASE). In the intermediate regime (damped SF), both coherence and collisions play a role. The cooperation number N_c gives the maximum number of atoms that can emit cooperatively. When the total number of excited atoms N is larger than N_c, the propagation effect is present and atoms undergo reabsorption and reemission processes. The SF emission has temporal ringing behavior. However, when $N < \sqrt{N_c}$, the propagation effect is negligible and pure SF is emitted. Figure 1 shows these various regimes determined by these parameters labeled ASE, damped SF, and SF (including strong-oscillatory SF, weak-oscillatory SF, and pure SF) [24]. With the parameters from the recent experiment [8] as $T_2 \sim 0.1$ ns, $T_1 = 0.108$ μs, $\lambda = 845$ nm, $L \sim 1$ cm, $A \sim 10^{-5}$ cm^2, and $n \sim 3 \times 10^{14}$ cm^{-3}, we obtain $\tau_r \approx 0.4$ ps, $\tau_D \approx 15$ ps, $\alpha L \approx 476$, and $N_c \approx 4 \times 10^7$. These parameters place the experiment of Ref. [8] in the strong-oscillatory SF regime.

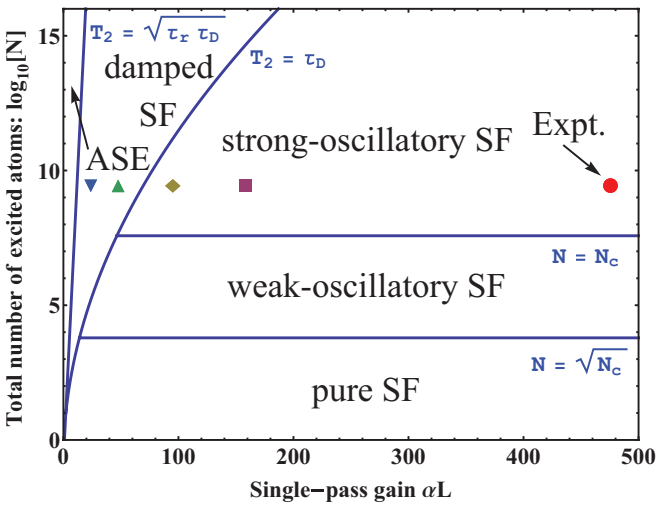

FIG. 1. (Color online) Regimes of N-atom cooperative spontaneous emission (adapted from Ref. [24]). The experimental parameters from Ref. [8] correspond to the strong-oscillatory SF regime (red circle). The four other points (purple square, yellow diamond, green triangle, and blue inverted triangle) correspond to four distinct sets of parameters used in simulations (see below).

In this paper we perform a detailed theoretical analysis of the recent experiment [8] and simulate strong-oscillatory temporal behavior of atmospheric oxygen emission. The coherence-brightened nature of this emission is revealed using picosecond pump excitation. We conclude that the measured spiky features in the emitted fields are due to coherence brightening and cannot be described by the rate equations or the pump noise.

II. THEORETICAL MODEL

In a recent experiment on atmospheric oxygen [8], a 10-ns, 226-nm pulse (propagating in the forward direction) dissociates oxygen molecules and is used as a pump in a three-level atomic oxygen system (see Fig. 2). Emission fields are generated from the $a \leftrightarrow b$ transition in both the forward and backward directions. As noted above, the field from the $b \leftrightarrow c$ transition can be coherently generated only in the forward direction. The backward field from the $b \leftrightarrow c$ transition is zero because of the phase mismatching with the forward pump field and the absence of the population inversion. The fields from the $a \leftrightarrow b$ transition have a wavelength of 845 nm and have been detected in both directions in the experiment [8]. The forward UV field at 130 nm from the $b \leftrightarrow c$ transition is also involved in the dynamics and affects the 845-nm fields, but has not been detected due to its strong absorption in air.

For our model, we use a pencil-like active medium, with a length of 1 cm and a cross-sectional area of 10^{-5} cm^2, as in the experiment. We assume that the atomic density in this active medium is constant at 10^{15} cm^{-3} (with population initially in the ground state). The two-photon excitation of the $a \leftrightarrow c$ transition by the pump pulse is treated as two excitation processes via two allowed transitions with the smallest detuning between the pump field and the transition from the ground level to an intermediate level. This intermediate level corresponds to the $3s\,^3S$ state (level b) in the atomic oxygen energy scheme. The detuning Δ is 6.1×10^{15} rad/s. The Rabi frequencies for the pump pulse coupled to the $a \leftrightarrow b$ and $b \leftrightarrow c$ transitions are $\Omega_{p1} = \wp_{ab}\mathcal{E}_p/\hbar$ and $\Omega_{p2} = \wp_{bc}\mathcal{E}_p/\hbar$, respectively, where $\wp_{ab}$ and $\wp_{bc}$ are the matrix elements of the electric dipole moment and $\mathcal{E}_p$ is the slowly varying

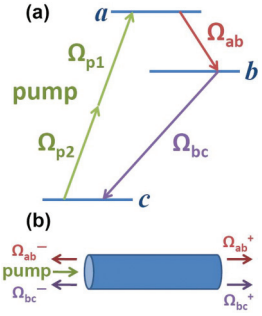

FIG. 2. (Color online) (a) Three-level energy diagram of an oxygen atom. Levels a, b, and c represent the states $3p\,^3P$, $3s\,^3S$, and $2p\,^3P$, respectively. (b) The pump pulse propagates in the forward direction. We consider fields from the $a \leftrightarrow b$ and $b \leftrightarrow c$ transitions in both the forward and backward directions in the theoretical model.

envelope amplitude with $E_p = \mathcal{E}_p e^{-i(\nu_p t - k_p z)} + \text{c.c.}$ Here E_p is the electric field, ν_p is the frequency, and k_p is the wave vector of the pump and z is taken to be positive for the forward propagation direction. The detailed derivation of the two-photon excitation is shown in Appendix A. The generated fields from the $a \leftrightarrow b$ and $b \leftrightarrow c$ transitions have both forward and backward contributions, which lead to the Rabi frequencies of $\Omega_{ab}^{+} e^{-i(\nu_{ab} t - k_{ab} z)} + \Omega_{ab}^{-} e^{-i(\nu_{ab} t + k_{ab} z)}$ and $\Omega_{bc}^{+} e^{-i(\nu_{bc} t - k_{bc} z)} + \Omega_{bc}^{-} e^{-i(\nu_{bc} t + k_{bc} z)}$, respectively. The plus and minus signs represent forward and backward propagation, respectively. Here Ω_{ab}^{+}, Ω_{ab}^{-}, Ω_{bc}^{+}, and Ω_{bc}^{-} are assumed to be slowly varying functions. These fields are coupled with the active atomic medium. The semiclassical Maxwell-Bloch (MB) equations are used to describe the physics of this three-level system. The phase-matching conditions are considered. The rotating-wave approximation (RWA) is used, so the terms coupling the fields and the polarization in the medium that are not phase matched are neglected. The detailed equations can be found in Appendix A.

III. PICOSECOND PUMP EXCITATION

In the recent experiment [8], a nanosecond laser pulse (with a full width at half maximum of ∼10 ns) was used to pump oxygen atoms. The density of the atomic oxygen in a pencil-like cylinder with the length $L = 1$ cm and cross-sectional area $A \sim 10^{-5}$ cm^2 is $n_a = 10^{15}$ cm^{-3}. The spontaneous emission rates are $\gamma_{ab} = 9.3 \times 10^6$ s^{-1} and $\gamma_{bc} = 1.97 \times 10^8$ s^{-1}. Hence the transition dipole moments are $\wp_{ab} \sim 1.38 \times 10^{-29}$ C m and $\wp_{bc} \sim 0.38 \times 10^{-29}$ C m. We first consider a shorter picosecond pump pulse to better understand the physics of the system. We choose a 20-ps pump pulse with the same order of the peak power as in the experiment (∼0.5 MW). Thus we can take the peak Rabi frequencies $\Omega_{p1} \sim 3.2 \times 10^{13}$ rad/s and $\Omega_{p2} \sim 8.4 \times 10^{12}$ rad/s and an effective Rabi frequency $\Omega_{\text{eff}} \equiv \Omega_{p1}\Omega_{p2}/\Delta \sim 4.4 \times 10^{10}$ rad/s. Doppler broadening is not included in this simulation because we assume that the collisional dephasing is the dominant relaxation process.

The pump pulse enters the medium at a time of 0.5 ns. The emission fields at 845-nm are generated in both the forward and backward directions. We fixed the boundary conditions for the 845-nm fields to be a small constant to play the role of a spontaneous emission source, but assume that there is no spontaneous emission source for the 130-nm field (the UV field is strongly absorbed in air). The depletion rate for the 845-nm fields is $\kappa \sim 1.5$ cm^{-1} due to the Rayleigh diffraction length. The simulation results of the temporal behavior of the 845-nm fields ($|\Omega_{ab}^{\pm}|$) for different collisional dephasing rates γ_{col} are shown in Fig. 3. Strong-oscillatory SF with large peak Rabi frequencies is seen in both the forward and backward directions when $\gamma_{\text{col}} = 10$ ns^{-1} [Fig. 3(a)]. The SF oscillations are damped and the intensity decreases for larger γ_{col}. The simulation results are consistent with the various regimes described in Fig. 1. The physics is clear with this short picosecond pump pulse excitation. The upper transition of the oxygen atom is inverted after this pump pulse. In the small dephasing rate limit, the inverted system radiates SF and generates a large quantum coherence via cooperation between ensemble atoms. After the population is transferred from the upper level to the middle level, the coherence plays an important role by producing a weaker radiation, which in turn transfers a portion of population back to the upper level. The small portion of the population in the upper level then

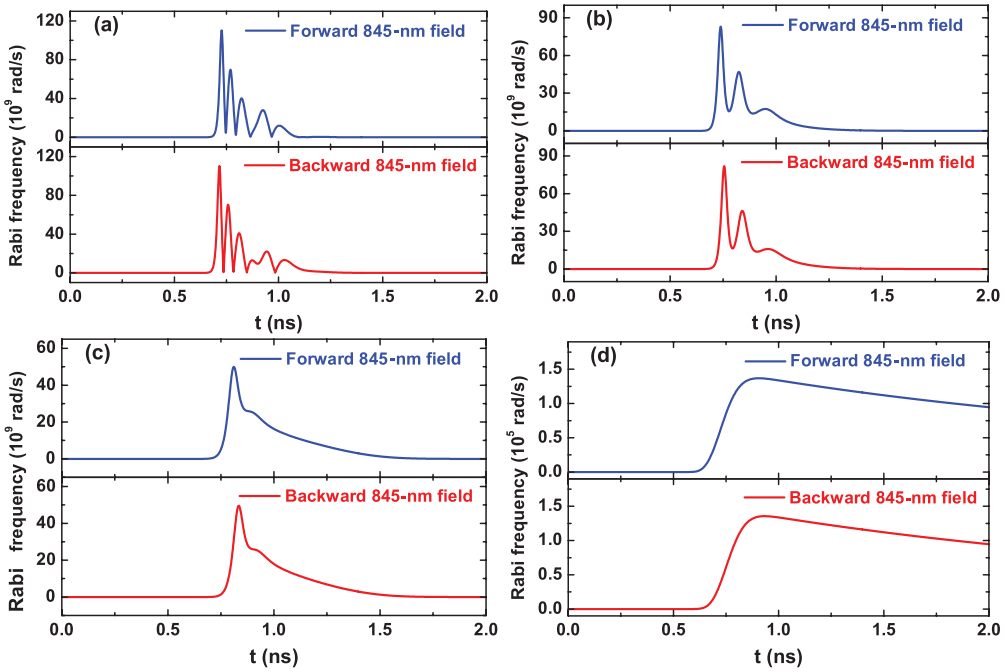

FIG. 3. (Color online) Temporal behavior of the 845-nm forward and backward fields generated by a 20-ps 226-nm pump pulse with different collisional dephasing rates: (a) $\gamma_{\text{col}} = 10$ ns^{-1} (leading to the regime labeled by the red circle in Fig. 1), (b) 30 ns^{-1} (labeled by purple square), (c) 50 ns^{-1} (labelled by yellow diamond), and (d) 100 ns^{-1} (labelled by green triangle).

continues to radiate cooperatively. This process repeats and results in the ringing (i.e., Burnham-Chiao ringing [29]) in Fig. 3(a). In the large dephasing rate limit [see Fig. 3(c)], the radiation generated by the inverted system produces a small amount of coherence because of the larger decoherence terms Γ_{ab} and Γ_{bc}. The amount of coherence is not large enough to reemit the field after the population moves to the middle level. However, there is a burst in the emission field because the process is still in the SF regime and the atoms radiate collectively. Nevertheless, with a significantly large dephasing rate (e.g., $\gamma_{\rm col} = 100\ {\rm ns}^{-1}$) [Fig. 3(d)], the inverted system cannot produce enough coherence so the radiation is closer to ASE than to SF. The difference between the forward and backward fields is not prominent in this regime. Phase-matching condition and the asymmetric scheme (i.e., forward and backward fields at the $a \leftrightarrow b$ and $b \leftrightarrow c$ transitions, but only a forward-propagating pump pulse) are the main reasons for the difference, which is discussed in detail in the following section. We find in this simulation with a simple short pump pulse that the atomic coherence is responsible for the spiky features.

IV. COMPARISON OF MAXWELL-BLOCH AND RATE EQUATIONS

In this section we match simulations more closely to the experiment [8] by using a nanosecond pump pulse. The long pump pulse makes the dynamics more complicated than in the preceding section. Namely, it keeps pumping the populations from the lower to the upper level, generating coherence between these two levels and coupling with the forward-propagating generated fields. We consider a 2-ns square-shaped pump pulse entering the medium at 0.5 ns and exiting at 2.5 ns, with the same peak Rabi frequency as in the preceding section.

The simulations were done using both the MB and the rate equations. It is well known that the rate equations can be derived from more general Maxwell-Bloch equations in the density-matrix treatment by the adiabatic approximation, which assumes that the transient part of the evolution of the atomic coherence can be neglected and the amplitude of such coherence follows adiabatically the changes of the population distribution [30]. This approximation eliminates the equations of the rapidly decaying dipole moment, such as Eqs. (A18) and (A19) in Appendix A, and describes the coherence terms as

$$\rho_{ab}^{\pm} = -\frac{i\Omega_{ab}^{\pm}(\rho_{aa} - \rho_{bb})}{\Gamma_{ab}}. \tag{5}$$

This approximation is valid only when the dephasing time is much shorter than the population relaxation time. Therefore, the coupling terms, such as the last term in Eq. (A18), can also be neglected because the large $\gamma_{\rm col}$ leads to a relatively small coherence term. This means that there are no coupling effects between the coherence and the field in two different transitions in the rate-equation picture. Now we insert the approximated coherence term back into the population equations, such as Eq. (A23), and the field propagating equations, such as Eq. (A26), and obtain the resulting differential rate equations as

$$\begin{aligned}\dot{\rho}_{bb} = {} & \gamma_{ab}\rho_{aa} - \gamma_{bc}\rho_{bb} + \frac{2|\Omega_{ab}^{+}|^2}{\Gamma_{ab}}(\rho_{aa} - \rho_{bb}) \\ & + \frac{2|\Omega_{ab}^{-}|^2}{\Gamma_{ab}}(\rho_{aa} - \rho_{bb}) - \frac{2|\Omega_{bc}^{+}|^2}{\Gamma_{bc}}(\rho_{bb} - \rho_{cc}) \\ & - \frac{2|\Omega_{bc}^{-}|^2}{\Gamma_{bc}}(\rho_{bb} - \rho_{cc}),\end{aligned} \tag{6}$$

$$\pm\frac{\partial\Omega_{ab}^{\pm}}{\partial z} + \frac{1}{c}\frac{\partial\Omega_{ab}^{\pm}}{\partial t} + \kappa\Omega_{ab}^{\pm} = \frac{\eta_{ab}\Omega_{ab}^{\pm}}{\Gamma_{ab}}(\rho_{aa} - \rho_{bb}), \tag{7}$$

and so on. The full set of rate equations is given in Appendix B with only populations and fields included. The atomic coherence is no longer included explicitly.

The simulation results using both the Maxwell-Bloch and the rate equations are shown in Fig. 4. In the small dephasing limit ($\gamma_{\rm col} = 10\ {\rm ns}^{-1}$), the resulting fields $|\Omega_{ab}^{\pm}|$ and the coherence $\rho_{ab}^{\pm}$ at the upper transition from the Maxwell-Bloch equations are shown in Figs. 4(a) and 4(b), respectively. Highly oscillatory SF radiation is generated similar to that in Fig. 3(a), but with a more complicated temporal profile. The long pump pulse continues to excite the population to the upper level, while the SF radiation depletes the excited atoms. The peak amplitude of the Rabi frequency is $\sim 10^{11}$ rad/s, which is consistent with the measurement in the experiment [8]. The forward field has a different shape from the backward field, as does the coherence $\rho_{ab}^{\pm}$. The real part of the coherence ρ_{ab}^{-}, which contributes to the backward field generation, is zero, but the real part of the coherence ρ_{ab}^{+}, which helps the forward field generation, is nonzero. This is the major cause of the difference between the forward and backward fields. The backward coherence (or field) is generated only by the population difference; however, the forward coherence can also result from the four-wave mixing. Namely, the two-photon excited coherence ρ_{ac} interacts with the radiation at the lower transition and contributes to the ρ_{ab}^{+} and the forward 845-nm field (and vice versa). In this simulation, a large amount of coherence ($\sim$0.1) at the $a \leftrightarrow b$ transition is produced. The fast change of the coherence makes it a nonadiabatic process. To prove this point, a simulation with the same decay rate but using the rate equations is shown in Figs. 4(c) and 4(d). Comparing the results with Figs. 4(a) and 4(b) from the Maxwell-Bloch equations, we see a different temporal behavior of the fields and the coherence. Therefore, the adiabatic approximation in the small dephasing limit ($\gamma_{\rm col} = 10\ {\rm ns}^{-1}$) is not valid and the rate equations give an incorrect result. The coherence effects play an important role when the Rabi frequency is larger than any relaxation rate. In this regime they can be described only by Maxwell-Bloch equations without the adiabatic approximation.

In contrast, in the large dephasing limit ($\gamma_{\rm col} = 200\ {\rm ns}^{-1}$), both the Maxwell-Bloch and rate equations give similar results for the fields and the coherence [see Figs. 4(e)–4(h)]. The amplitude of the Rabi frequency at the 845-nm emission is $\sim 10^{7}$ rad/s, which is much smaller than the dephasing rate. In this regime, since the coherence effects are not important, the adiabatic approximation works well and the simplified rate equations are adequate to describe the physical process.

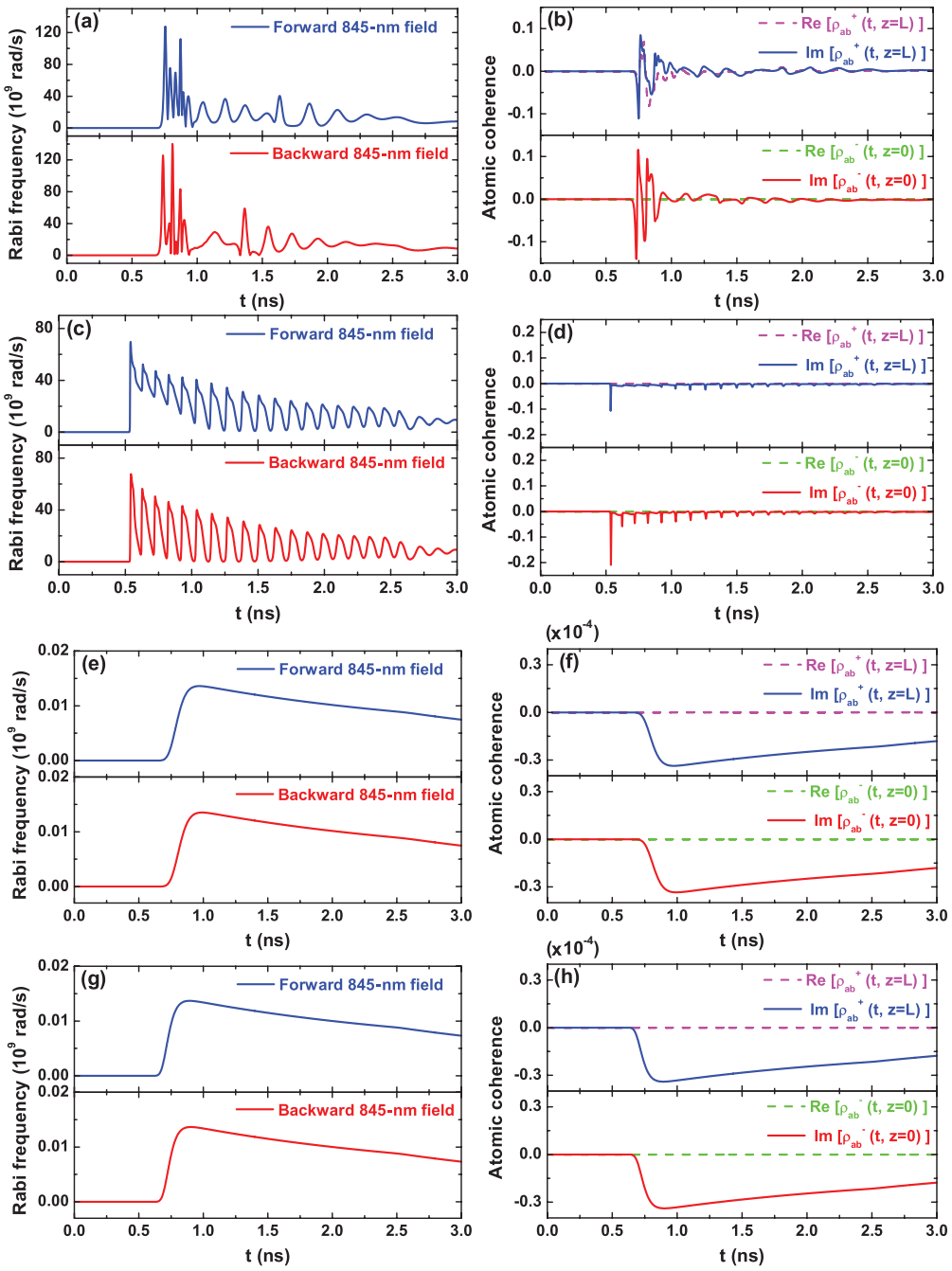

FIG. 4. (Color online) Temporal behavior of the fields $\Omega_{ab}^{\pm}$ and the atomic coherence $\rho_{ab}^{\pm}$ pumped by a nanosecond pulse simulated using the Maxwell-Bloch (MB) and rate equations for different dephasing rates $\gamma_{\rm col} = 10\ {\rm ns}^{-1}$ (leading to the regime labeled by the red circle in Fig. 1) and $\gamma_{\rm col} = 200\ {\rm ns}^{-1}$ (labeled by blue inverted triangle in Fig. 1): (a) and (b) MB equations with $\gamma_{\rm col} = 10\ {\rm ns}^{-1}$, (c) and (d) rate equations with $\gamma_{\rm col} = 10\ {\rm ns}^{-1}$, (e) and (f) MB equations with $\gamma_{\rm col} = 200\ {\rm ns}^{-1}$, and (g) and (h) rate equations with $\gamma_{\rm col} = 200\ {\rm ns}^{-1}$. The coherence in the simulations with the rate equations was calculated using Eq. (5).

In Fig. 5 we show two-dimensional plots of the generated 845-nm forward and backward fields inside the active medium with the parameters the same as in Fig. 4(a). The fields are plotted for the position z from 0 to 1 cm and the time t from 0.7 to 1 ns. We show the evolution of the spiky features of the fields in space and time. We notice that the forward and backward fields dominate in different regions; namely, the forward field is much larger in the region $z > 0.5$ cm and the backward field in $z < 0.5$ cm. The fields evolve from a broad peak to spiky oscillations with changing position because the single-pass gain [Eq. (1)] increases with the propagation distance. The nonadiabatic coherence makes the fields evolve fast in both the temporal and spatial domains.

V. NOISY NANOSECOND PUMP PULSE EXCITATION

From the discussion above we find that the atomic coherence plays a role in the spiky features of the generated

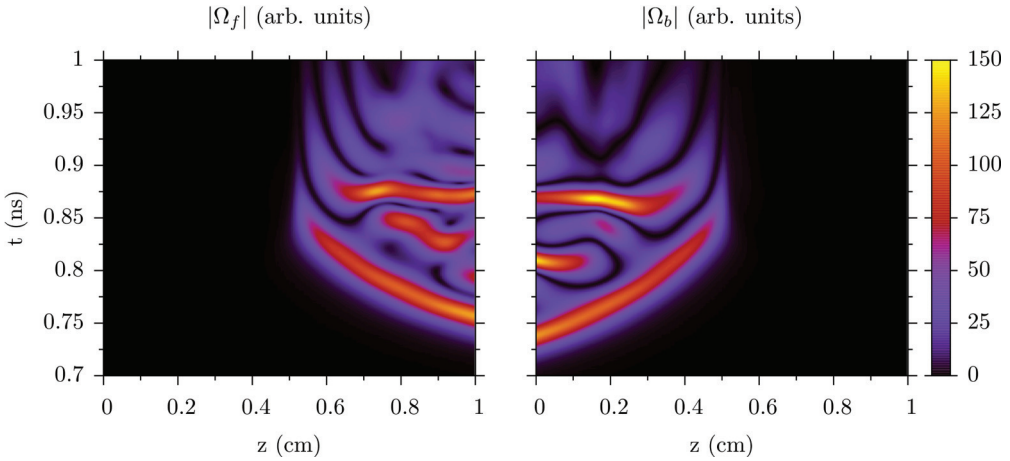

FIG. 5. (Color online) Generated 845-nm forward (left) and backward (right) fields dependent on time and position. The parameters are the same as those in Fig. 4(a).

845-nm SF emission. It is necessary to consider other possible mechanisms that might produce the spiky temporal behavior of the fields in the experiment. One possibility is a noisy pump pulse. In this section we keep all the parameters the same as those used in Figs. 3(a), 4(a), and 4(b), which are close to the experimental parameters, but we change the pump pulse shape.

The simulation results are shown in Fig. 6. In Fig. 6(a) we added small-amplitude noisy fluctuations to the square pump pulse that was used in Fig. 4(a). The simulation results show that the forward and backward 845-nm fields have different shapes than the fields generated from a square pump pulse and the pump shape itself. In the case of large-amplitude noisy fluctuations in the square pump pulse [as in Fig. 6(b)], the generated fields have different pulse shapes, which are uncorrelated with the pump fluctuations. Therefore, we conclude that, in the SF regime, the spikiness of the SF pulse is primarily due to the fast collective damping rate and the coherence effects (as in the Burnham-Chiao ringing that was discussed in Sec. III). The noise in the pump pulse plays a role and modifies the spikes in the emission field temporal behavior (and in some regimes, the noisy pump features lead to similar temporal behavior of the generated fields), but it is not the primary reason for the creation of the spikes [8].

VI. CONCLUSION

We presented a detailed derivation of the theoretical model for the coherence-brightened oxygen lasing experiment [8]. Strong-oscillatory SF temporal behavior has been confirmed in the simulations. We conclude that the spiky features of the emission fields are mainly due to coherence effects. The rate equations are not adequate to describe this behavior. The pump noise is not responsible for the spiky temporal behavior of the 845-nm fields. This theoretical study supports the experimental demonstration of a coherence-brightened laser source in air, in the Dicke sense [9].

ACKNOWLEDGMENTS

The authors thank Anatoly A. Svidzinsky for helpful discussions. We acknowledge the support of the National Science Foundation Grants No. EEC-0540832 (MIRTHE

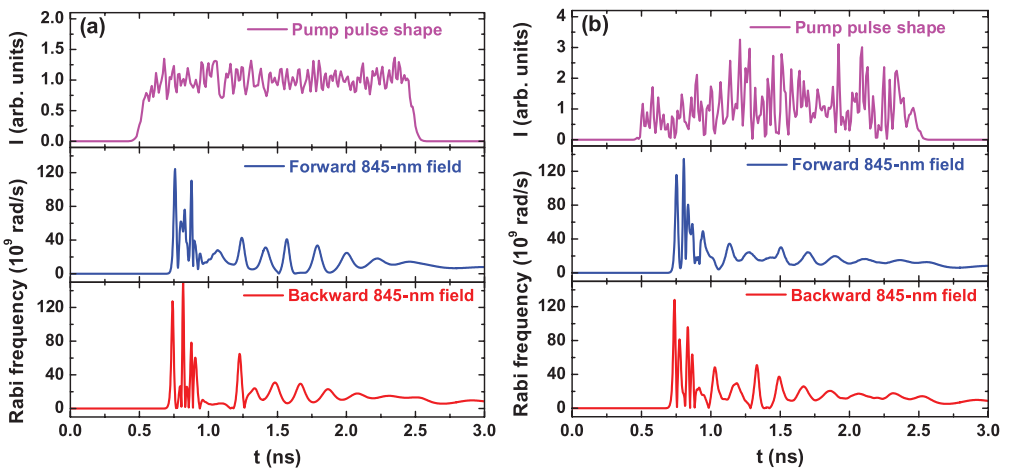

FIG. 6. (Color online) Temporal profiles of the 845-nm forward and backward fields generated by different noisy pump shapes (shown in the first row).

ERC) and No. PHY-1068554, the Office of Naval Research, and the R.A. Welch Foundation (Awards No. A-1261 and No. A-1547). L.Y. and A.J.T. were supported by the Herman F. Heep and Minnie Belle Heep Texas A&M University Endowed Fund held and administered by the Texas A&M Foundation.

APPENDIX A: MAXWELL-BLOCH EQUATIONS

Here we discuss the derivation of the two-photon excitation in detail and list the full set of density-matrix equations. Using the slowly varying approximation and the RWA and the assumption that the pump Rabi frequencies $\Omega_{p1}(t,z)$ and $\Omega_{p2}(t,z)$ are positive real functions, the Hamiltonian in the interaction picture reads

$$\begin{aligned} H_I = &-\hbar\Omega_{p1}e^{-i\Delta t+ik_pz}|a\rangle\langle b| - \hbar\Omega_{p2}e^{i\Delta t+ik_pz}|b\rangle\langle c| \\ &- \hbar(\Omega_{ab}^{+}e^{ik_{ab}z} + \Omega_{ab}^{-}e^{-ik_{ab}z})|a\rangle\langle b| - \hbar(\Omega_{bc}^{+}e^{ik_{bc}z} \\ &+ \Omega_{bc}^{-}e^{-ik_{bc}z})|b\rangle\langle c| + \text{H.c.} \end{aligned} \tag{A1}$$

The density-matrix equations for the coherence are

$$\begin{aligned} \dot{\rho}_{ab} = &-\Gamma_{ab}\rho_{ab} - i(\Omega_{ab}^{+}e^{ik_{ab}z} + \Omega_{ab}^{-}e^{-ik_{ab}z})(\rho_{aa} - \rho_{bb}) \\ &- i\Omega_{p1}e^{-i\Delta t+ik_pz}(\rho_{aa} - \rho_{bb}) \\ &- i(\Omega_{bc}^{+*}e^{-ik_{bc}z} + \Omega_{bc}^{-*}e^{ik_{bc}z})\rho_{ac} - i\Omega_{p2}^{*}e^{-i\Delta t-ik_pz}\rho_{ac}, \end{aligned} \tag{A2}$$

$$\begin{aligned} \dot{\rho}_{bc} = &-\Gamma_{bc}\rho_{bc} - i(\Omega_{bc}^{+}e^{ik_{bc}z} + \Omega_{bc}^{-}e^{-ik_{bc}z})(\rho_{bb} - \rho_{cc}) \\ &- i\Omega_{p2}e^{i\Delta t+ik_pz}(\rho_{bb} - \rho_{cc}) \\ &+ i(\Omega_{ab}^{+*}e^{-ik_{ab}z} + \Omega_{ab}^{-*}e^{ik_{ab}z})\rho_{ac} + i\Omega_{p1}^{*}e^{i\Delta t-ik_pz}\rho_{ac}, \end{aligned} \tag{A3}$$

$$\begin{aligned} \dot{\rho}_{ac} = &-\Gamma_{ac}\rho_{ac} + i(\Omega_{ab}^{+}e^{ik_{ab}z} + \Omega_{ab}^{-}e^{-ik_{ab}z})\rho_{bc} \\ &+ i\Omega_{p1}e^{-i\Delta t+ik_pz}\rho_{bc} \\ &- i(\Omega_{bc}^{+}e^{ik_{bc}z} + \Omega_{bc}^{-}e^{-ik_{bc}z})\rho_{ab} - i\Omega_{p2}e^{i\Delta t+ik_pz}\rho_{ab}, \end{aligned} \tag{A4}$$

where the dephasing rates are $\Gamma_{ab} = \frac{1}{2}(\gamma_{ab} + \gamma_{bc}) + \gamma_{\text{col}}$, $\Gamma_{bc} = \frac{1}{2}\gamma_{bc} + \gamma_{\text{col}}$, and $\Gamma_{ac} = \frac{1}{2}\gamma_{ab} + \gamma_{\text{col}}$, with γ_{col} being the collisional dephasing rate and γ_{ab} and γ_{bc} the spontaneous decay rates at the $a \leftrightarrow b$ and $b \leftrightarrow c$ transitions, respectively. Expressing the coherence as a sum of the slow and fast varying terms (the latter oscillating at a frequency as the detuning Δ)

$$\rho_{ab} = \sigma_{ab} + u_{ab}e^{-i\Delta t}, \tag{A5}$$

$$\rho_{bc} = \sigma_{bc} + u_{bc}e^{i\Delta t}, \tag{A6}$$

plugging those two definitions into Eqs. (A2)–(A4), and using the RWA to neglect the fast oscillating terms we obtain

$$\begin{aligned} \dot{\sigma}_{ab} = &-\Gamma_{ab}\sigma_{ab} - i(\Omega_{ab}^{+}e^{ik_{ab}z} + \Omega_{ab}^{-}e^{-ik_{ab}z})(\rho_{aa} - \rho_{bb}) \\ &- i(\Omega_{bc}^{+*}e^{-ik_{bc}z} + \Omega_{bc}^{-*}e^{ik_{bc}z})\rho_{ac}, \end{aligned} \tag{A7}$$

$$\begin{aligned} \dot{u}_{ab} = &-(\Gamma_{ab} - i\Delta)u_{ab} - i\Omega_{p1}e^{ik_pz}(\rho_{aa} - \rho_{bb}) \\ &- i\Omega_{p2}^{*}e^{-ik_pz}\rho_{ac}, \end{aligned} \tag{A8}$$

$$\begin{aligned} \dot{\sigma}_{bc} = &-\Gamma_{bc}\sigma_{bc} - i(\Omega_{bc}^{+}e^{ik_{bc}z} + \Omega_{bc}^{-}e^{-ik_{bc}z})(\rho_{bb} - \rho_{cc}) \\ &+ i(\Omega_{ab}^{+*}e^{-ik_{ab}z} + \Omega_{ab}^{-*}e^{ik_{ab}z})\rho_{ac}, \end{aligned} \tag{A9}$$

$$\begin{aligned} \dot{u}_{bc} = &-(\Gamma_{bc} + i\Delta)u_{bc} - i\Omega_{p2}e^{ik_pz}(\rho_{bb} - \rho_{cc}) \\ &+ i\Omega_{p1}^{*}e^{-ik_pz}\rho_{ac}, \end{aligned} \tag{A10}$$

$$\begin{aligned} \dot{\rho}_{ac} = &-\Gamma_{ac}\rho_{ac} + i(\Omega_{ab}^{+}e^{ik_{ab}z} + \Omega_{ab}^{-}e^{-ik_{ab}z})\sigma_{bc} + i\Omega_{p1}e^{ik_pz}u_{bc} \\ &- i(\Omega_{bc}^{+}e^{ik_{bc}z} + \Omega_{bc}^{-}e^{-ik_{bc}z})\sigma_{ab} - i\Omega_{p2}e^{ik_pz}u_{ab}. \end{aligned} \tag{A11}$$

Because the detuning Δ in Eqs. (A8) and (A10) is much larger than any relaxation process, we assume that the terms u_{ab} and u_{bc} reach steady state quickly. Therefore, we write them as

$$u_{bc} = \frac{-\Omega_{p2}e^{ik_pz}(\rho_{bb} - \rho_{cc}) + \Omega_{p1}^{*}e^{-ik_pz}\rho_{ac}}{\Delta - i\Gamma_{bc}}, \tag{A12}$$

$$u_{ab} = \frac{\Omega_{p1}e^{ik_pz}(\rho_{aa} - \rho_{bb}) + \Omega_{p2}^{*}e^{-ik_pz}\rho_{ac}}{\Delta + i\Gamma_{ab}}. \tag{A13}$$

Plugging these two solutions into Eq. (A11) with the assumption that $\Delta \gg \Gamma_{ij}$, we find

$$\begin{aligned} \dot{\rho}_{ac} = &-\Gamma_{ac}\rho_{ac} + i\frac{|\Omega_{p1}|^2 - |\Omega_{p2}|^2}{\Delta}\rho_{ac} \\ &- i\frac{\Omega_{p1}\Omega_{p2}}{\Delta}e^{i2k_pz}(\rho_{aa} - \rho_{cc}) \\ &+ (\Omega_{ab}^{+}e^{ik_{ab}z} + \Omega_{ab}^{-}e^{-ik_{ab}z})\sigma_{bc} \\ &- (\Omega_{bc}^{+}e^{ik_{bc}z} + \Omega_{bc}^{-}e^{-ik_{bc}z})\sigma_{ab}. \end{aligned} \tag{A14}$$

Next we express the coherence as slowly varying terms with position z,

$$\sigma_{ab} = \rho_{ab}^{+}e^{ik_{ab}z} + \rho_{ab}^{-}e^{-ik_{ab}z}, \tag{A15}$$

$$\sigma_{bc} = \rho_{bc}^{+}e^{ik_{bc}z} + \rho_{bc}^{-}e^{-ik_{bc}z}, \tag{A16}$$

and

$$\rho_{ac} \to \rho_{ac}e^{i2k_pz}. \tag{A17}$$

Keeping in mind that the phase-matching condition gives $2k_p - k_{ab} - k_{bc} = 0$, we plug Eqs. (A15)–(A17) back into Eqs. (A7), (A9), and (A14) and use the RWA to remove the terms with fast oscillation with z. (The treatment of the density-matrix equations for the population is the same as for ρ_{ac}). Then we derive the full set of the density-matrix equations, which is summarized in the following:

$$\dot{\rho}_{ab}^{+} = -\Gamma_{ab}\rho_{ab}^{+} - i\Omega_{ab}^{+}(\rho_{aa} - \rho_{bb}) - i\Omega_{bc}^{+*}\rho_{ac}, \tag{A18}$$

$$\dot{\rho}_{ab}^{-} = -\Gamma_{ab}\rho_{ab}^{-} - i\Omega_{ab}^{-}(\rho_{aa} - \rho_{bb}), \tag{A19}$$

$$\dot{\rho}_{bc}^{+} = -\Gamma_{bc}\rho_{bc}^{+} - i\Omega_{bc}^{+}(\rho_{bb} - \rho_{cc}) + i\Omega_{ab}^{+*}\rho_{ac}, \tag{A20}$$

$$\dot{\rho}_{bc}^{-} = -\Gamma_{bc}\rho_{bc}^{-} - i\Omega_{bc}^{-}(\rho_{bb} - \rho_{cc}), \tag{A21}$$

$$\begin{aligned} \dot{\rho}_{ac} = &-\left[\Gamma_{ac} - i\frac{|\Omega_{p1}|^2 - |\Omega_{p2}|^2}{\Delta}\right]\rho_{ac} \\ &- i\frac{\Omega_{p1}\Omega_{p2}}{\Delta}(\rho_{aa} - \rho_{cc}) + i\Omega_{ab}^{+}\rho_{bc}^{+} - i\Omega_{bc}^{+}\rho_{ab}^{+}, \end{aligned} \tag{A22}$$

$$\dot{\rho}_{aa} = -\gamma_{ab}\rho_{aa} + \left(i\Omega_{ab}^{+}\rho_{ba}^{+} + i\Omega_{ab}^{-}\rho_{ba}^{-} + i\frac{\Omega_{p1}\Omega_{p2}}{\Delta}\rho_{ca} + \text{c.c.}\right), \quad \text{(A23)}$$

$$\dot{\rho}_{bb} = \gamma_{ab}\rho_{aa} - \gamma_{bc}\rho_{bb} + (-i\Omega_{ab}^{+}\rho_{ba}^{+} - i\Omega_{ab}^{-}\rho_{ba}^{-} + i\Omega_{bc}^{+}\rho_{cb}^{+} + i\Omega_{bc}^{-}\rho_{cb}^{-} + \text{c.c.}), \quad \text{(A24)}$$

$$\rho_{aa} + \rho_{bb} + \rho_{cc} = 1. \quad \text{(A25)}$$

We neglect Doppler broadening in the simulation because the collisional dephasing rate is the dominating relaxation process in the current experiment [8]. The Maxwell-Bloch equations read

$$\pm\frac{\partial\Omega_{ab}^{\pm}}{\partial z} + \frac{1}{c}\frac{\partial\Omega_{ab}^{\pm}}{\partial t} + \kappa\Omega_{ab}^{\pm} = i\eta_{ab}\rho_{ab}^{\pm}, \quad \text{(A26)}$$

$$\pm\frac{\partial\Omega_{bc}^{\pm}}{\partial z} + \frac{1}{c}\frac{\partial\Omega_{bc}^{\pm}}{\partial t} = i\eta_{bc}\rho_{bc}^{\pm}, \quad \text{(A27)}$$

where $\eta_{ij} = \frac{3}{8\pi}n_a\lambda_{ij}^2\gamma_{ij}$ is the field-atom coupling constant, n_a is the atomic density, and κ is the decay rate of the 845-nm field due to the Rayleigh diffraction limit.

APPENDIX B: RATE EQUATIONS

The rate equations are derived from the density-matrix equations (A18)–(A27) by the adiabatic approximation. This approximation eliminates the equations of the rapidly decaying dipole moment. Namely, Eqs. (A18)–(A22) become

$$0 \simeq -\Gamma_{ab}\rho_{ab}^{\pm} - i\Omega_{ab}^{\pm}(\rho_{aa} - \rho_{bb}), \quad \text{(B1)}$$

$$0 \simeq -\Gamma_{bc}\rho_{bc}^{\pm} - i\Omega_{bc}^{\pm}(\rho_{bb} - \rho_{cc}), \quad \text{(B2)}$$

$$0 \simeq -\left[\Gamma_{ac} - i\frac{|\Omega_{p1}|^2 - |\Omega_{p2}|^2}{\Delta}\right]\rho_{ac} - i\frac{\Omega_{p1}\Omega_{p2}}{\Delta}(\rho_{aa} - \rho_{cc}), \quad \text{(B3)}$$

where the transient parts of coherence $\rho_{ab}^{\pm}$ and $\rho_{bc}^{\pm}$ can be neglected, and they follow adiabatically from the population difference [30]. The full set of rate equations may be derived by plugging the results of Eqs. (B1)–(B3) into all the rest of the density-matrix equations [Eqs. (A23)–(A27)]

$$\dot{\rho}_{aa} = -\gamma_{ab}\rho_{aa} - \frac{2|\Omega_{ab}^{+}|^2 + 2|\Omega_{ab}^{-}|^2}{\Gamma_{ab}}(\rho_{aa} - \rho_{bb}) - \frac{2\Gamma_{ac}|\Omega_{p1}\Omega_{p2}|^2}{\Gamma_{ac}^2\Delta^2 + (|\Omega_{p1}|^2 - |\Omega_{p2}|^2)^2}(\rho_{aa} - \rho_{cc}), \quad \text{(B4)}$$

$$\dot{\rho}_{bb} = \gamma_{ab}\rho_{aa} - \gamma_{bc}\rho_{bb} + \frac{2|\Omega_{ab}^{+}|^2 + 2|\Omega_{ab}^{-}|^2}{\Gamma_{ab}}(\rho_{aa} - \rho_{bb}) - \frac{2|\Omega_{bc}^{+}|^2 + 2|\Omega_{bc}^{-}|^2}{\Gamma_{bc}}(\rho_{bb} - \rho_{cc}), \quad \text{(B5)}$$

$$\rho_{aa} + \rho_{bb} + \rho_{cc} = 1, \quad \text{(B6)}$$

$$\pm\frac{\partial\Omega_{ab}^{\pm}}{\partial z} + \frac{1}{c}\frac{\partial\Omega_{ab}^{\pm}}{\partial t} + \kappa\Omega_{ab}^{\pm} = \frac{\eta_{ab}\Omega_{ab}^{\pm}}{\Gamma_{ab}}(\rho_{aa} - \rho_{bb}), \quad \text{(B7)}$$

$$\pm\frac{\partial\Omega_{bc}^{\pm}}{\partial z} + \frac{1}{c}\frac{\partial\Omega_{bc}^{\pm}}{\partial t} = \frac{\eta_{bc}\Omega_{bc}^{\pm}}{\Gamma_{bc}}(\rho_{bb} - \rho_{cc}). \quad \text{(B8)}$$

[1] A. M. Zheltikov, M. N. Shneider, A. A. Voronin, A. V. Sokolov, and M. O. Scully, Laser Phys. Lett. **9**, 68 (2012).
[2] J. Liu, J. Dai, S. L. Chin, and X.-C. Zhang, Nat. Photonics **4**, 627 (2010).
[3] Y. V. Rostovtsev, Z. E. Sariyanni, and M. O. Scully, Phys. Rev. Lett. **97**, 113001 (2006).
[4] L. Yuan, K. E. Dorfman, A. M. Zheltikov, and M. O. Scully, Opt. Lett. **37**, 987 (2012).
[5] P. R. Hemmer, R. B. Miles, P. Polynkin, T. Siebert, A. V. Sokolov, P. Sprangle, and M. O. Scully, Proc. Natl. Acad. Sci. USA **108**, 3130 (2011).
[6] L. Yuan, A. A. Lanin, P. K. Jha, A. J. Traverso, D. V. Voronine, K. E. Dorfman, A. B. Fedotov, G. R. Welch, A. V. Sokolov, A. M. Zheltikov, and M. O. Scully, Laser Phys. Lett. **8**, 736 (2011).
[7] A. Dogariu, J. B. Michael, M. O. Scully, and R. B. Miles, Science **331**, 442 (2011).
[8] A. J. Traverso, R. Sanchez-Gonzalez, L. Yuan, K. Wang, D. V. Voronine, A. M. Zheltikov, Y. Rostovtsev, V. A. Sautenkov, A. V. Sokolov, S. W. North, and M. O. Scully, Proc. Natl. Acad. Sci. USA **109**, 15185 (2012).
[9] R. H. Dicke, in *The Coherence Brightened Laser*, edited by P. Grivet and N. Bloembergen, Proceedings of the Third International Congress on Quantum Electronics (Dunod Éditeur, Paris, and Columbia University Press, New York, 1964), p. 35.
[10] R. H. Dicke, Phys. Rev. **93**, 99 (1954).
[11] N. Skribanowitz, I. P. Herman, J. C. MacGillivray, and M. S. Feld, Phys. Rev. Lett. **30**, 309 (1973).
[12] J. C. MacGillivray and M. S. Feld, Phys. Rev. A **14**, 1169 (1976).
[13] R. Bonifacio, F. Hopf, P. Meystre, and M. Scully, *Laser Induced Fusion and X-Ray Laser Studies* (Addison-Wesley, Reading, MA, 1976), pp. 487–556.
[14] M. Gross and S. Haroche, Phys. Rep. **93**, 301 (1982).
[15] V. V. Zheleznyakov, V. V. Kocharovskiĭ, and Vi. V. Kocharovskiĭ, Sov. Phys. Usp. **32**, 835 (1989).
[16] J. H. Brownell, X. Lu, and S. R. Hartmann, Phys. Rev. Lett. **75**, 3265 (1995).
[17] A. I. Lvovsky, Ph.D. thesis, Columbia University, 1998.
[18] W. R. Garrett, Phys. Rev. Lett. **70**, 4059 (1993).
[19] L. Yuan and A. A. Svidzinsky, Phys. Rev. A **85**, 033836 (2012).
[20] P. W. Hoff, H. A. Haus, and T. J. Bridges, Phys. Rev. Lett. **25**, 82 (1970).
[21] L. W. Hillman, J. Krasiński, R. W. Boyd, and C. R. Stroud, Jr., Phys. Rev. Lett. **52**, 1605 (1984).
[22] C. Y. Wang, L. Diehl, A. Gordon, C. Jirauschek, F. X. Kärtner, A. Belyanin, D. Bour, S. Corzine, G. Höfler, M. Troccoli, J. Faist, and F. Capasso, Phys. Rev. A **75**, 031802 (2007).
[23] L. Allen and J. H. Eberly, *Optical Resonance and Two Level Atoms* (Dover, New York, 1987).
[24] J. J. Maki, M. S. Malcuit, M. G. Raymer, R. W. Boyd, and P. D. Drummond, Phys. Rev. A **40**, 5135 (1989).

[25] R. Friedberg and S. R. Hartmann, Phys. Lett. **37A**, 285 (1971).
[26] R. Friedberg and S. R. Hartmann, Phys. Rev. A **13**, 495 (1976).
[27] D. Polder, M. F. H. Schuurmans, and Q. H. F. Vrehen, Phys. Rev. A **19**, 1192 (1979).
[28] F. T. Arecchi and E. Courtens, Phys. Rev. A **2**, 1730 (1970).
[29] D. C. Burnham and R. Y. Chiao, Phys. Rev. **188**, 667 (1969).
[30] C. L. Tang, *Fundamentals of Quantum Mechanics for Solid State Electronics and Optics* (Cambridge University Press, New York, 2005), p. 199.